Aquaculture 564 (2023) 739067

Contents lists available at ScienceDirect

Aquaculture

journal homepage: www.elsevier.com/locate/aquaculture

Integration of host-pathogen functional genomics data into the chromosome-level genome assembly of turbot (*Scophthalmus maximus*)

Oscar Aramburu, Andrés Blanco, Carmen Bouza *, Paulino Martínez

Department of Zoology, Genetics and Physical Anthropology, Faculty of Veterinary, Universidade de Santiago de Compostela, Campus of Lugo, 27002 Lugo, Spain

ARTICLE INFO

Keywords:
Scophthalmus maximus
Differentially expressed genes
QTL
ROH
Disease resistance

ABSTRACT

Disease resilience is of utmost relevance for turbot aquaculture. Several infective diseases, covering a broad spectrum from viruses, bacteria to different parasites, have been identified by industry. Since they increase mortality rates, reduce feed conversion ratios and slow down growth rate, genetic breeding programs for increasing disease resilience are recognized as a useful alternative for controlling pathologies. For this, knowledge of the genetic basis underlying resilience using genomic tools is essential to develop the best effective breeding strategies. In the present study, we compiled the existing genomic information generated in the last decade to construct an integrated atlas of candidate genes and genomic regions involved in pathogen resistance against the main turbot industrial pathogens (*Aeromonas salmonicida, Philasterides dicentrarchi, Enteromyxum scophthalmi* and the VHS virus) within the chromosome-level turbot genome assembly recently released. Information comprehends reannotated differentially expressed genes (DEG) in different tissues along temporal series, QTL markers associated with important productive traits (disease resistance and growth) and signatures of domestic or wild selection, represented by runs of homozygosity (ROHi) islands and outlier markers for divergent selection. Most genetic features were successfully relocated in the turbot assembly including 81.1% of the total DEGs, plus all QTL markers, ROHi and outlier markers. The updated annotation of DEGs for resistance to each pathology demonstrated significant changes. While the new annotation of 53–83% of the DEGs was coherent with the original, roughly 10–24% showed imprecise annotations in both assembly versions, ~5% lost their original annotation and 2–24% were now annotated. Functional enrichment revealed mostly functions related to immune response, such as chemotaxis, apoptosis regulation, leukocyte differentiation, cell adhesion, iron homeostasis and vascular permeability. Some DEGs, such as *celsr1a* (cadherin EGF LAG seen-pass G-type receptor 1), *fgg* (fibrinogen gamma chain) and *c1qtnf9* (C1q and TNF related 9) were found near pathogen-associated QTL markers. Also, some shared DEGs for resistance to all pathogens were positioned near QTL markers or ROHi, such as *hamp* (hepcidin-1), *plg* (plasminogen) and a fibrinogen alpha chain-like gene. Overall, our results provide an integrative insight into the genetic architecture of turbot response to a range of pathogens that could prove useful for future genomic studies to benefit aquaculture breeding programs.

1. Introduction

The turbot (*Scophthalmus maximus*) is an economically important flatfish for European and Chinese aquaculture. Breeding programs for improving growth rate began in Europe in the 1990s and are currently in the 6th generation of selection (Martínez et al., 2021). The production of cultured turbot was roughly 60,000 tons in 2018, with China as the main producer (50,000 tons; Ma et al., 2021) followed by Spain (8000 t in 2019; APROMAR, 2021).

As it is frequent in animals under intensive production, pathologies constitute one of the main problems of turbot aquaculture. Disease resilience is a key research goal, since around 40% of the worldwide aquaculture production losses are due to pathologies (Owens, 2012). Diseases not only compromise the viability of farmed animals, but also reduce feed conversion ratio and growth, and further increase production costs for their control. The furunculosis, caused by the gram-

Abbreviations: AS, *Aeromonas salmonicida*; PD, *Philasterides dicentrarchi*; VHSV, Viral Haemorrhagic Septicaemia Virus; ES, *Enteromyxum scophthalmi*; QTL, Quantitative trait loci; DEG, Differentially expressed gene/s; ROHi, Run of Homozygosity Island; GO, Gene Onthology; B/D, Balancing / Divergent selection; D/A, Domestication / Artificial selection.

* Corresponding author.
E-mail address: mcarmen.bouza@usc.es (C. Bouza).

https://doi.org/10.1016/j.aquaculture.2022.739067
Received 28 July 2022; Received in revised form 8 November 2022; Accepted 14 November 2022
Available online 17 November 2022

negative bacteria *Aeromonas salmonicida* (AS), the scuticociliatosis, caused by the ciliated protozoan *Philasterides dicentrarchi* (PD), the enteromyxosis, caused by the parasitic myxozoan *Enteromyxum scophthalmi* (ES), and the viral haemorrhagic septicemia, caused by the rhabdovirus VHS, are among the main infective diseases affecting farmed turbot (Millán et al., 2011; Pardo et al., 2012; Díaz-Rosales et al., 2012; Robledo et al., 2014; Ronza et al., 2016).

There are no decisive treatments for controlling these diseases, even though some vaccines have already been developed or tested to fight against furunculosis (Ellis, 1997), scuticociliatosis (Iglesias et al., 2001; León-Rodríguez et al., 2012) and VHSV (Pereiro et al., 2016), and some chemotherapeutics have been applied for preventing scuticociliatosis (Paramá et al., 2004, Paramá et al., 2005; Budiño et al., 2012). In other cases, such as enteromyxosis, there are no treatments, thus the only option is prevention by disinfection or early detection of the parasite for culling of the infected tanks to prevent its spread (Ronza et al., 2019).

Developing resilient strains through selective breeding is an increasingly applied measure to control diseases at farms (Gjedrem and Rye, 2018; Elaswad and Dunham, 2018). Resilience against specific diseases affecting aquaculture species have shown significant heritabilities suggesting its potential for genetic improvement (Ødegård et al., 2011). Despite the complex nature of disease resilience, the advances in genomic technologies have made it possible to dissect genetic variation underlying these traits and quantitative trait loci (QTL) explaining a significant proportion of the phenotypic variance have been identified for their application on breeding programs (Munang'andu et al., 2018; Fraslin et al., 2020). Furthermore, sometimes it was possible to disentangle the different components of resilience by assessing the resistance to be infected and the tolerance for survival once infected (Saura et al., 2019; Knap and Doeschl-Wilson, 2020).

Single nucleotide polymorphisms (SNPs) and microsatellites are the genetic markers commonly used for genomic screening to look for association with target traits (Fraslin et al., 2020; Houston et al., 2020). Many QTL and closely linked associated markers for disease resilience traits in aquaculture have been discovered throughout the years, and more recently by applying Restriction Site Associated DNA Sequencing (RAD-seq) and SNP arrays methodologies for genome-wide association studies (GWAS) (Yue et al., 2014; Gutierrez et al., 2018; Peñaloza et al., 2021; Garcia et al., 2021). In turbot, QTL explaining a significant proportion of the phenotypic variance have been identified for growth rate and resistance to the main pathologies affecting farming (Sánchez-Molano et al., 2011; Sciara et al., 2018; Rodríguez-Ramilo et al., 2011, 2013, 2014). The availability of highly dense genetic maps and refined genome assemblies (Figueras et al., 2016; Maroso et al., 2018) allowed mining for candidate genes underlying QTL regions and developing GWAS for disentangling genetic variation underlying resilience to PD (Saura et al., 2019).

Moreover, detection of differentially expressed genes (DEG) across the infection process in immune-related tissues is another strategy commonly used to elucidate the genes and biological functions/pathways associated with immune response to infections. Such studies have been addressed in turbot during the last decade, using different functional genomics approaches. The first studies were addressed with custom microarrays, and thousands of gene expression profiles associated with fluorescence signals on gene-specific probes were used to understanding complex biological functions (Park et al., 2009). In the case of turbot, a custom oligo-microarray enriched for immune genes was designed (Millán et al., 2010) and used for identifying DEG and enriched functions regarding response against AS (Millán et al., 2011), PD (Pardo et al., 2012; Valle et al., 2020) and VHSV (Díaz-Rosales et al., 2012; Pereiro et al., 2014). Later RNA-seq, a more sensitive and accurate technique that can distinguish expression profiles of paralogous genes and identify gene-associated single nucleotide polymorphisms (Ronza et al., 2019), was applied on infections with the intestinal parasite *E. scophthalmi* during late (Robledo et al., 2014) and early (Ronza et al., 2016) enteromyxosis stages, as well as to revisit the study of infections with PD (Valle et al., 2020) and AS (Librán-Pérez et al., 2022) with this new technology.

Recently, Aramburu et al. (2020) took advantage of the amount of genomic information existing in turbot to check for selective sweeps around previously reported signatures of selection and QTL for productive traits in wild and farmed populations (Martínez, 2016; do Prado et al., 2018a, 2018b) through characterization of Runs of Homozygosity islands (ROHi; Metzger et al., 2015) and heterozygosity across its genome. The availability of a highly contiguous chromosome-level genome assembly based on long-read sequencing (97% of the assembly integrated in the $n = 22$ turbot chromosomes; Martínez et al., 2021) opens the opportunity, as suggested by these authors, for integrating all previous genomic information related to productive traits and adaptive variation, and further updating functional annotation. Integrating structural and functional genomic data into the latest high-quality genomes is essential to support gene localizations and annotations enabling the application of functional genomics studies in livestock (Tuggle et al., 2006; Hadlich et al., 2021).

In this study, taking as reference the updated chromosome-level assembly of turbot (Martínez et al., 2021), we aimed to: i) revise genomic location and functional annotation of DEG sequences derived from microarray probes and RNAseq data; ii) relocate QTL markers and ROHi to construct an integrated atlas of meaningful genomic regions related to resistance to pathologies and showing suggestive signals of selection; iii) apply this information to suggest or confirm key genomic regions related to resistance to a broad spectrum of pathogens affecting turbot industry; iv) to identify genes or pathways activated in response to either specific diseases or shared among different pathologies that could aid to identify biomarkers for disease control.

2. Material and methods

2.1. Data source

The genomic data integrated in this work has been gathered from different studies from the last decade, where marker sequences are available to revisit genome alignments and functional annotation analysis (Fig. 1). They include QTL markers for resistance to *A. salmonicida* (AS), *P. dicentrarchi* (PD) and the Viral Haemorrhagic Septicaemia Virus (VHSV) published by Rodríguez-Ramilo et al. (2011, 2013 and 2014, respectively) and Saura et al. (2019, PD only). Also, QTL information for growth rate was reported by Sánchez-Molano et al. (2011) and Sciara et al. (2018). Data for other QTL and trait associated markers such as sex determination, impact of domestication and balancing/divergent selection were published by Martínez et al. (2009) and do Prado et al. (2018a, 2018b). Sets of accessible DNA sequences for differentially expressed genes (DEG) in response to infections by AS, PD, VHSV and *Enteromyxum scophthalmi* (ES) were published by Millán et al. (2011), Pardo et al. (2012), Díaz-Rosales et al. (2012), Robledo et al. (2014), Ronza et al. (2016) and Librán-Pérez et al. (2022). Finally, a study on Runs of Homozygosity islands (ROHi) and signatures of selective sweeps was carried out by Aramburu et al. (2020).

2.2. Raw functional transcriptomic data

Sequence data comprised microarray oligo-probes (~60 bp), mostly representing tags of the 3′ untranslated region (UTR) (Millán et al., 2010), from a total of 471 and 221 DEG detected in spleen, liver, and head kidney in response to intraperitoneal challenges with AS (Millán et al., 2011) and PD (Pardo et al., 2012), respectively. Another 127 oligo-probes (Millán et al., 2010), corresponding to 65 DEG in head kidney from VHSV intraperitoneally infected turbot (Díaz-Rosales et al., 2012), were also included. On the other hand, we also considered DNA sequences for 4295, 1173 and 2056 DEG derived from RNAseq data detected in head kidney, liver, and pyloric caeca in response to severe (Robledo et al., 2014) and early (Ronza et al., 2016) ES infection stages,

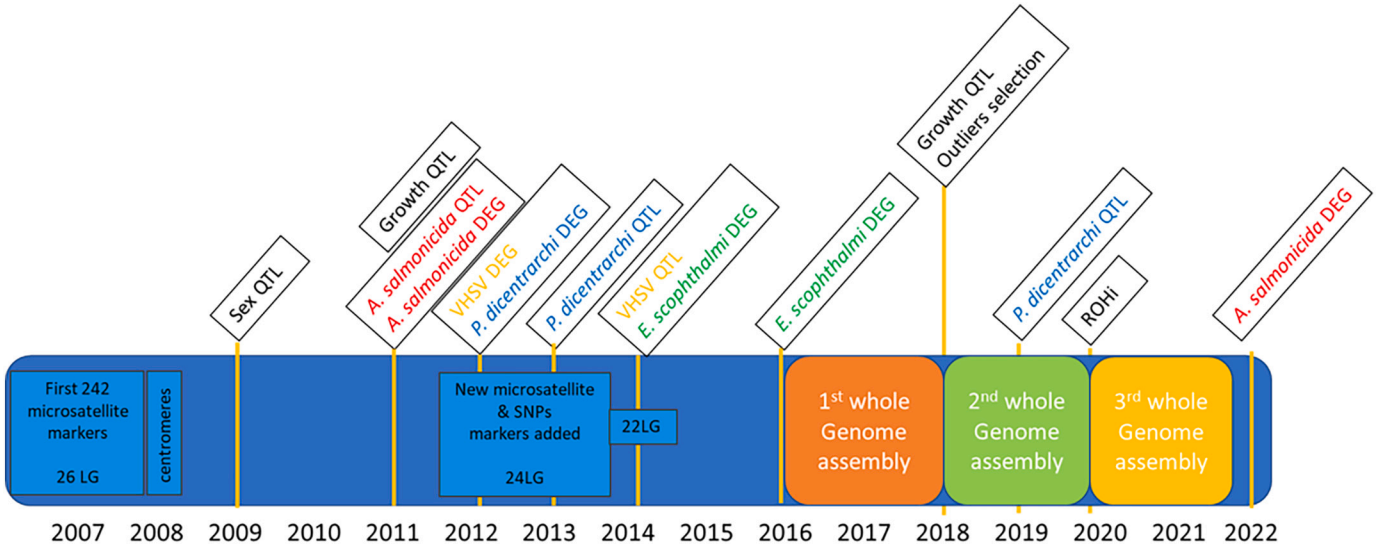

Fig. 1. Timeline of the most relevant genomic studies (yellow labels) carried out on disease resistance and other traits in *Scophthalmus maximus* from 2007 to 2022 related to the different genetic maps (blue squares) and genome assemblies released. (For interpretation of the references to colour in this figure legend, the reader is referred to the web version of this article.)

and head kidney in response to AS infection (Librán-Pérez et al., 2022), respectively.

2.3. Genome alignment

Oligo-microarray probes were aligned against the updated chromosome-level turbot genome assembly (ASM1334776v1; Martínez et al., 2021) using Bowtie 1.3.0. (Langmead et al., 2009). Allowed mismatches were set to a maximum of 3 (parameter "-v 3") and, if a given oligo-probe showed multiple hits, only that with the least number of mismatches was retained (parameters" -a –best –strata"). The alignments were catalogued as single-hits (one match) or multiple-hits (two or more hits with the same number of mismatches), the later likely pointing to paralogous sequences, which were discarded for further analyses due to doubtful expression data. The genome position of each single-hit oligo was compared with the position of nearby genes in the turbot genome, and only when oligos overlapped with annotated genes were considered as oligos inside genes. Those oligos located <2 kb away (up / downstream) of an annotated gene were considered as nearby oligos.

RNAseq-derived DEG sequences were first aligned against the latest turbot transcriptome (ASM1334776v1) using ncbi-BLAST 2.11 with the blastn -megablast alignment option (default parameters; Morgulis et al., 2008). For each sequence, only the best alignment (e-value < e-50; best bitscore) was retained; when several alignments showed the same bitscore, all of them were considered. Given those parameters, each successful alignment was catalogued as single-hit (only one match) or multiple-hit (two or more matches). The unaligned sequences against the turbot transcriptome were then blasted against its genome, using the same parameters and filtering steps outlined before. On top of that, we searched for overlapping between each DEG single-hit sequence and an annotated gene in the turbot genome.

Finally, gene annotations recorded for single-hit oligos and cDNA reads in the original studies were updated using the latest turbot genome annotation (Martínez et al., 2021).

2.4. Shared DEG across infective diseases

The list of DEG for each pathogen was compared to identify shared DEG in response to different pathogens, with special focus on those shared among all the four diseases. DEG were further subdivided by tissue to make comparisons for head kidney (AS, PD, VHSV and ES), spleen (AS, PD and ES) and liver (AS and PD) expression profiles.

2.5. QTL and ROHi positioning

The positions of 49 ROHi (Aramburu et al., 2020) identified in the previous turbot chromosome-level assembly (ASM318616v1; Maroso et al., 2018) were transferred to the last version (ASM1334776v1; Martínez et al., 2021). These ROHi are suggestive signatures of domestication or selection generated in breeding programs during more than 30 years of turbot farming (Martínez, 2016). Similarly, the 165 highest associated QTL-markers or related to adaptive variation in wild or farm populations were relocated in the updated turbot genome assembly. These markers were associated with one or more productive traits: 9 markers were associated with resistance to AS (Rodríguez-Ramilo et al., 2011), 40 to PD (Rodríguez-Ramilo et al., 2013; Saura et al., 2019) and 16 to VHSV (Rodríguez-Ramilo et al., 2014); 52 markers were associated with growth (Sánchez-Molano et al., 2011) and 4 with sex determination (Martínez et al., 2009); further, 21 and 53 outlier markers showing signatures of balancing or divergent (B/D) selection in the wild (Vilas et al., 2010, 2015; do Prado et al., 2018a), and domestication/artificial (D/A) selection in farm populations (do Prado et al., 2018b), were also included. The position of ROHi and QTL-associated markers was compared to those of DEG to search for DEG inside ROHi or positioned at <250 kb up/downstream of a certain QTL marker (here onwards, DEG "close to" QTL markers).

2.6. Categorizing updated annotations

The original and updated annotation of DEG was compared and catalogued as "conserved", "inaccurate", "lost" or "new" based on whether both annotations were the same (conserved), were too loose (inaccurate), the original annotation was lost after realignment (lost), or previously unannotated genes were annotated (new). The full lists of DEG for resistance were analysed using ShinyGO v.075 (Ge et al., 2020) to retrieve functional enrichment GO terms related to Biological Process, with an FDR cut-off of $P < 0.05$.

3. Results

3.1. Genome alignment and annotation

On average, 84.5% DEG sequences could be repositioned in the updated turbot assembly and 64.4% of the original annotations were conserved in the new genome (ASM1334776v1) (Supplementary Table 2). For the oligo-probe based studies on resistance to AS, PD and VHSV, between 69.3 and 79.0% were catalogued as single-hits (Table 1). Most of the VHS-DEG conserved their annotations (83.7%), the remaining genes showing inaccurate annotation, either in the original study or in the updated assembly. For AS and PD the annotation ratios were quite similar, although lower than those observed for VHSV: on average above half of the DEG conserved their annotations (56.05%), with 24.1% on average showing inaccurate annotations. In the updated assembly, some previously unannotated DEG for AS and PD were annotated (average 15.4%), and a few DEG lost their annotation (average 4.5%) (Table 1, Supplementary Table 2). Regarding the RNAseq studies on early and severe response to ES, between 74.5 and 92.5% of the DEG were catalogued as single-hits, respectively. More conserved annotations were found for severe (72.5%) than for early (53.5%) enteromyxosis (Table 1). Newly annotated ES-DEG were more frequent on early (24.1%) than severe (5.5%) enteromyxosis, with similar ratios for inaccurate and lost annotations (average: 17.5% and 4.6%, respectively). Finally, for the RNAseq study on AS infection, 76.5% of the DEG were catalogued as single-hits, with most of them (83.8%) conserving their annotation in the updated genome, with almost even proportions between newly annotated (2.37%) and lost annotations (3.08%) (Table 1, Supplementary Table 2).

3.2. Shared DEG across infective diseases

The analysis of common DEG across the studied infective diseases unveiled a total of 709 shared DEG between at least two diseases, six of them being regulated in all the four diseases examined: *aat-like (*alpha-1 antitrypsin), *plg (*Plasminogen), *hamp* (hepcidin-1), *C3-like* (complement C3-like), *gapdh* (glyceraldehyde-3-phosphate dehydrogenase) and *fga-like* (fibrinogen alpha chain-like) (Fig. 2, Fig. 3, Supplementary Fig. 1). In total, 74 DEG were shared between different disease trios, especially between AS-ES-PD (65), and much lower when VHSV was included in the comparisons: AS-ES-VHSV (5) and AS-PD-VHSV (4). The other 629 shared by pairs were: AS-ES (542), AS-PD (43), ES-PD (25), ES-VHSV (10), AS-VHSV (6) and PD-VHSV (3), again showing the more specific response against the virus.

Looking at tissue profiles, only head kidney was analysed in the four diseases and showed a total of 210 shared DEG; only one gene (*hamp*) shared between all diseases, 12 by trios and by pairs. For spleen (not analysed for VHSV), a total of 89 DEG were shared, 27 by the three diseases studied (AS, ES and PD), and the other 62 by pairs. Finally for liver, only studied in AS and PD infections, 30 DEG were shared. (Fig. 2, Table 2A and 2B, Supplementary Table 3, Supplementary Fig. 1).

The DEG list for AS from Librán-Pérez et al. (2022) was compared against the information from Millán et al. (2011) for the same condition (Head Kidney, 24 hpi; total of 41 DEGs). A total of 15 genes were differentially expressed in both studies, representing 35.59% of Millán et al.'s head kidney 24 hpi sublist.

3.3. ROHi and QTL positioning

The lists of ROHi and QTL-associated markers were repositioned against the updated turbot genome assembly (Fig. 4). All the 49 previously identified ROHi in a domestic turbot population (Aramburu et al., 2020) were positioned to the updated genome assembly (Supplementary Table 4A), confirming their previous chromosomal distribution. While the size of 44 ROHi was similar to that described in the previous assembly (89.8%, ±10% of the original extension), three of them showed striking differences, two of them being much bigger than in the previous assembly (ROHi_07 and ROHi_08 in C04; 800% and 94% bigger, respectively) and the other much smaller (ROHi_30 in C13, only 0.7% of the original extension) (Maroso et al., 2018; Aramburu et al., 2020).

The full list of QTL-associated markers was transferred to the updated assembly; these markers belonged to studies with diverse experimental approaches, even when targeting the same traits, such as those for response to PD (Rodríguez-Ramilo et al., 2011; Saura et al., 2019) and for growth (Sánchez-Molano et al., 2011; Sciara et al., 2018). All turbot chromosomes contained at least two markers considering all the traits evaluated (Supplementary Table 4B). The average number per-chromosome was 7.4 ranging from 14 QTL-markers (C02 and C08) to 2 (C11). Most QTL markers associated with VHSV resistance were grouped in chromosomes C01 (4), C07 (5), C10 (3) and C21 (3); for PD resistance, even further clustering was observed, with most markers located in C03 (8), C08 (6), C10 (6) and C17 (9). Finally for AS resistance, no relevant marker clustering was found in any chromosome, with only C08 (3) and C10 (2) showing more than one AS-associated marker.

3.4. DEG vs QTL-associated markers and ROHi

Starting from the microarray data, a total of 23 DEG in response to AS were located inside 12 ROHi, and other 60 DEG were close to 49 QTL-associated markers for resistance to AS (2 QTLs), PD (12) and VHSV (3), growth (15) and sex determination (2), or outlier loci for B/D selection (15) and D/A selection (7) (Supplementary Table 5). The two DEG detected near AS-QTL were *celsr1a* (cadherin EGF LAG seven-pass G-type receptor 1; Sma-USC256, C02) and *CFH-like* (complement factor H-like; SmaUSC-E30, C12) (Table 3).

As outlined before, a significant higher number of DEGs was detected from RNAseq data and thus within ROHi; a total of 113 DEG in response to AS were located inside 31 ROHi, and other 248 DEG were close to 121 QTL-associated markers for resistance to AS (4 QTLs), PD (27) and VHSV (12), growth (38) and sex determination (2), or outlier loci for B/D selection (40) and D/A selection (15). The 9 DEG detected near AS-QTL were *paqr5-like* (membrane progestin receptor gamma-B-like), near Sma-USC47 in C05; *mttp* (microsomal triglyceride transfer protein),

Table 1
Summary of the alignment and annotation of the pathogen-specific differentially expressed genes (DEG) lists comparing the original studies with results from the updated turbot genome assembly (ASM1334776v1; Martínez et al., 2021).

Pathogen*	Initial DEG set	Single-hit genes (%)	Total updated DEG	"Conserved" annotation (%)	"Inaccurate" annoration (%)	"New" annotation (%)	"Lost" annotation (%)
AS 2011	471	372 (79.0)	362	205 (55.0)	90 (24.1)	62 (16.6)	16 (4.3)
AS 2022	2056	1575 (76.6)	1560	1307(83.8)	168 (10.8)	37 (2.4)	48 (3.1)
PD	221	170 (76.9)	162	97 (57.1)	41 (24.1)	24 (14.1)	8 (4.7)
VHSV	127	88 (69.3)	49	41 (83.7)	8 (16.3)	–	–
ES (early)	1174	874 (74.5)	826	442 (53.5)	152 (18.4)	199 (24.1)	33 (4.0)
ES (severe)	4295	3972 (92.5)	3480	2524 (72.5)	580 (16.7)	191 (5.5)	185 (5.3)

* Original studies: AS-*A.salmonicida* (Millán et al., 2011; Librán-Pérez et al., 2022); PD-*P. dicentrarchi* (Pardo et al., 2012); VHSV-Viral haemorrhagic septicaemia virus (Díaz-Rosales et al., 2012), ES-*E. scophthalmi* (Ronza et al., 2016; Robledo et al., 2014).

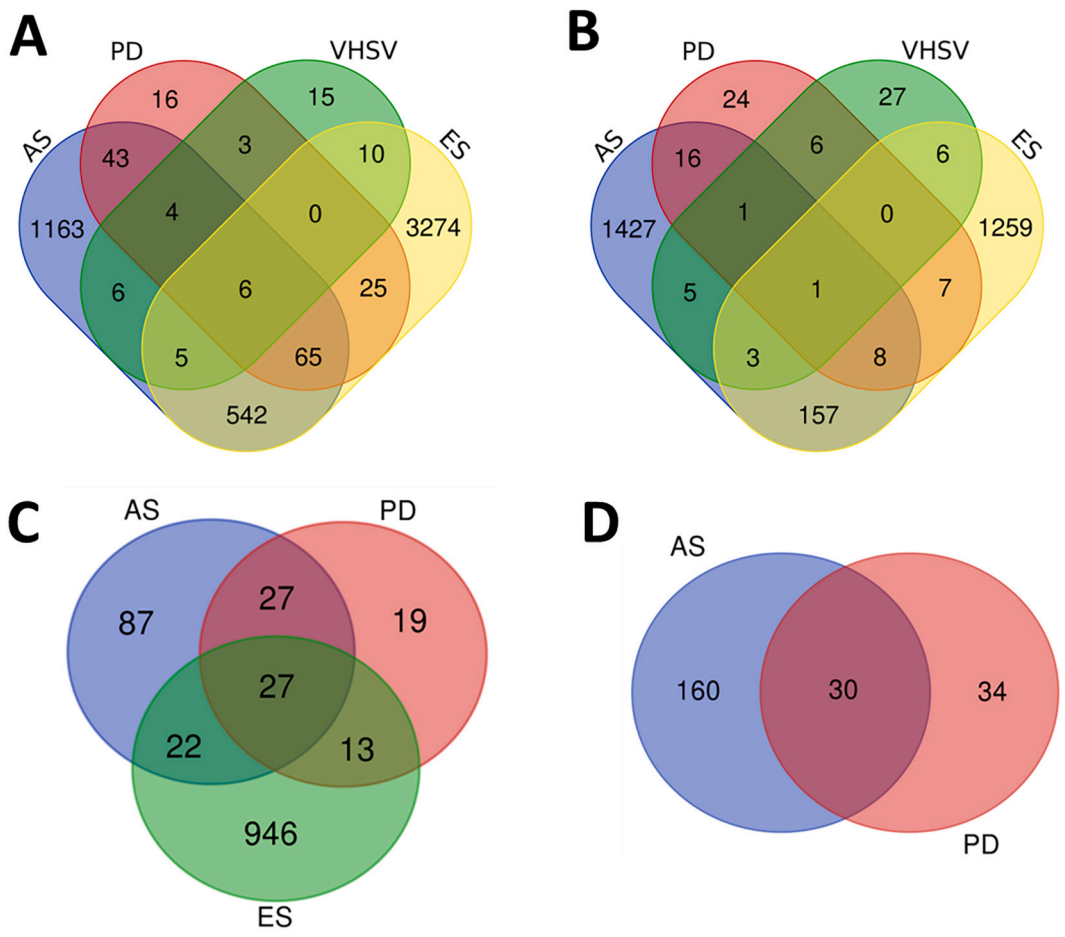

Fig. 2. Venn diagrams for differentially expressed genes (DEG) in response to *Aeromonas salmonicida* (AS), *Philasterides dicentrarchi* (PD), Viral Haemorrhagic Septicaemia Virus (VHSV) and *Enteromyxum scophthalmi* (ES) in *Scophthalmus maximus*. A) Full list of DEG; B) head kidney DEG; C) Spleen DEG; D) Liver DEG.

dnaja1 (DnaJ heat shock protein family member A1), *aptx* (aprataxin), *odam* (odontogenic ameloblast associated molecule), *mdt30-like* (glutamine/asparagine-rich protein mdt30-like) and *scpp5* (secretory calcium-binding phosphoprotein 5), all 6 near SmaUSC-E23 in C08; and *apoh-like* (beta-2-glycoprotein 1-like) and *pld5* (phospholipase D family member 5), near SmaUSC-E41 and Sma-USC21, respectively (C08).

A total of 15 DEG in response to PD were located inside 10 ROHi, whereas 29 were close to 29 QTL-associated markers for resistance to PD (4), AS (1) and VHSV (1), growth (7) and sex (2), or B/D selection (9) and D/A selection (5) markers (Supplementary Table 5). Three DEG were identified near PD associated QTL markers: *pdia2* (protein disulfide-isomerase A2; SmaUSC-E36, C08) and *fgg*; sm5s20_3350768, C08); and *sgk1* (Serum/glucocorticoid regulated kinase 1; Sma-USC38 and sm5s47_538662, C20) (Table 3).

Three DEG for response to VHSV were inside ROHi, while ten DEG were located near 10 QTL-associated markers for resistance to VHSV (2), growth (4) and sex (1)), or B/D selection (5) and D/A selection (1) markers (Supplementary Table 5). The four DEG found close to VHSV QTL-markers were *hamp* (; Sma-USC109, C01), and *rpl21* (ribosomal protein L21), *c1qtnf9* (C1q and TNF related protein 9) and *plcpi-like* (leukocyte cysteine proteinase inhibitor 1), all three located at C21 close to Sma-USC91 (Table 3).

A total of 308 DEG in response to ES (271 and 60 for early and severe enteromyxosis, respectively; 23 shared) were located inside 39 ROHi (37 severe, 22 early, 20 shared); and 619 DEG (507 for severe, 110 for early, 50 shared) were close to 157 QTL-associated markers (152 severe, 91 early, 86 common). (Supplementary Table 5). For severe enteromyxosis, DEG were distributed close to QTL-markers associated with AS (9), PD (35), VHSV (16), growth (47), sex (4), or B/D selection (50) and D/A selection (19) markers. For early enteromyxosis, the distribution was among AS (5), PD (13) and VHSV (8), growth (22) and sex (1), or B/D selection (19) and D/A selection (10) outlier loci. Given the lack of QTL studies for ES resistance in turbot, we looked at ES-DEG near QTL associated to other pathogens, which unveiled some interesting genes such as *hamp* near a VHSV-QTL (Sma-USC109, C01 or *sgk1* near a PD-QTL (Sma-USC38, C20) (Table 3). The same was done for growth associated markers, and genes such as *cyp2k1-like* and *cyp2k4-like* (cytochrome P450 2 k1-like and 2 k4-like; Sma-USC252, C20), and *cdx1b* (caudal type homeobox 1 b) and *oatx* (organic anion transporter X) both near SmaUSC-E40 at C04, all of them also located inside ROHi.

3.5. Functional enrichment of DEG

The full lists of positioned DEG in response to AS, PD and ES were characterized through functional enrichment (Supplementary Table 6). Most of the recovered GO terms for Biological Process (FDR < 0.05) fitted to general categories related to disease response, that had been reported in their respective studies for AS and PD (14 categories) and ES (5 categories). In a few cases, significant GO terms not allocated in those categories, such as those associated with the development of the eye, lateral line and fin/appendages, and brain/heart morphogenesis, were detected. Although no similar comparison could be made for VHSV due to the lack of similar classifications, two major functions were unveiled among the twenty significantly enriched GO terms retrieved: metabolic process and transport.

For AS, a total of 205 significantly enriched GO terms were detected

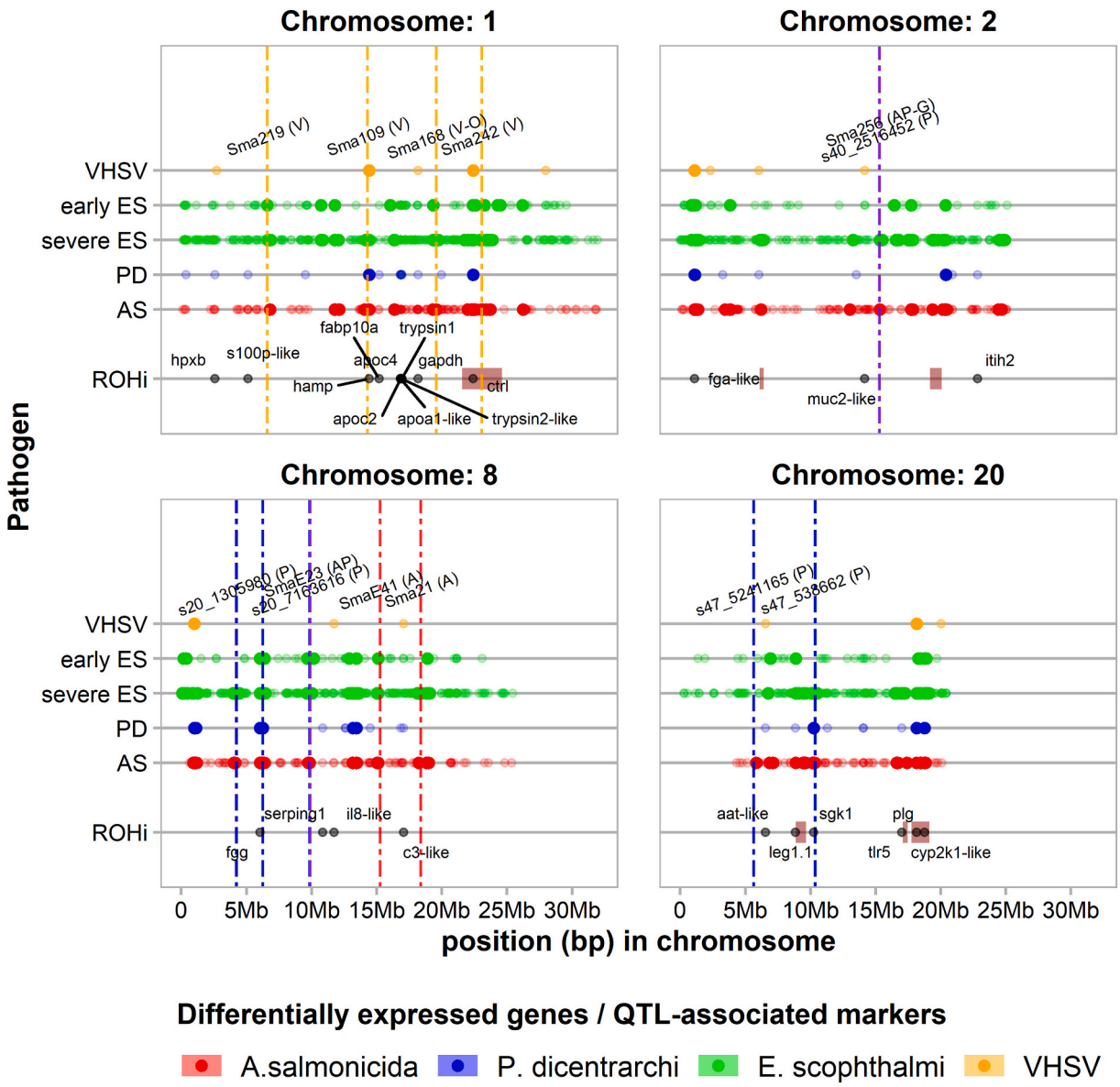

Fig. 3. Positioning of selected shared differentially expressed genes (DEG; gray dots; labelled) in response to three to four pathogens studied respect to disease-associated QTL markers (vertical dotted lines) and ROH islands (ROHi, pink squares) in chromosomes C01, C02, C08 and C20 of *Scophthalmus maximus*. Each labelled row represents DEG in that chromosome in response to *Aeromonas salmonicida* (AS), *Philasterides dicentrarchi* (PD), Viral Haemorrhagic Septicaemia Virus (VHSV) and *Enteromyxum scophthalmi* (ES). Each QTL is labelled with the associated marker name and coded for the diseases/traits in brackets (A, AS; P, PD; V, VHSV; G, growth, O, selection outlier). Gene descriptions: *hpxb* (hemopexin), *s100p-like* (protein S100-P-like), *fabp10a* (fatty acid-binding protein 10-A), *apoc4* (apolipoprotein C-IV), *apoc2* (apolipoprotein C-II), *apoa1-like* (apolipoprotein A-I-like), *ctrl* (chymotrypsin-like protease CTRL-1), *itih2* (inter-alpha-trypsin inhibitor heavy chain H2), *serping1* (plasma protease C1 inhibitor), *leg1.1* (liver-enriched gene 1, tandem duplicate 1). (For interpretation of the references to colour in this figure legend, the reader is referred to the web version of this article.)

related to response to stimulus, metabolic process, apoptosis, erythrocyte differentiation, hemostasis and coagulation, and hepatocyte and connective tissue development and eye/lateral line development gathering the oligo and RNAseq dataset information. A total of 88 GO terms were obtained for the PD dataset, most related to response to stimulus, endocytosis, cell proliferation / differentiation (particularly leukocytes) hemostasis and coagulation, stress response, cartilage and bone growth, iron transport and ROS regulation. For early (245 terms) and severe (248 terms) enteromyxosis, most terms were related to transport, response to stimulus, coagulation and hemostasis, and blood cell differentiation. Early enteromyxosis showed more GO terms related to epithelium development, muscle development and locomotion, cell adhesion, response to starvation, whereas severe enteromyxosis showed more terms related to regeneration, cell migration, stress, growth and lipid metabolic process.

4. Discussion

In this study, an integrated up-to-date genomic atlas of functional transcriptomic features related to resistance for major turbot aquaculture diseases was accomplished. Previously reported differentially expressed genes (DEG) derived from microarray in response to *Aeromonas salmonicida* (AS; Millán et al., 2011), *Philasterides dicentrarchi* (PD; Pardo et al., 2012) and the Viral Haemorrhagic Septicaemia virus (VHSV; Díaz-Rosales et al., 2012), and RNAseq data in response to *Enteromyxum scophthalmi* (ES; Robledo et al., 2014; Ronza et al., 2016) and AS (Librán-Pérez et al., 2022) were reannotated and mapped to the updated and contiguous genome assembly of the species (Martínez et al.,

Table 2A
Selection of the most relevant shared differentially expressed genes (DEG) across infections with *Aeromonas salmonicida* (AS), *Philasterides dicentrarchi* (PD), *Enteromyxum scophthalmi* (ES) and the VHS virus regardless of tissue in *Scophthalmus maximus*. DEG shared in response to at least three of the pathogens are shown with their start position (in Mb) in the respective chromosome (C). In bold, newly annotated genes; underlined nearby genes to the oligos of DEG in the microarray analysis.

Gene	Position (Mb)	Gene	Position (Mb)	Gene	Position (Mb)
AS-PD-ES-VHSV		AS-PD-ES (cont)		AS-PD-ES (cont)	
hamp	C01:14.42	itih2	C02:22.83	serpinc1	C12:0.43
gapdh	C01:18.18	***slc7a1-like***	C03:8.28	***fetub***	C12:2.83
fga-like	C02:1.11	vtnb	C04:5.48	cfh-like	C12:3.79
C3-like	C08:17.05	f9b	C04:6.77	cp	C12:4.64
aat-like	C20:6.55	cfb-like	C04:11.44	agxta	C12:20.98
plg	C20:18.15	mmp13-like	C04:18.93	dusp1	C13:15.38
AS-PD-VHSV		ctrb-like	C05:1.84	slc40a1	C14:4.23
ctrl1-like	C01:22.39	hp	C05:10.80	etv5a	C14:21.57
rtp3-like	C12:10.53	isp2-like	C05:18.86	habp2-like	C15:13.68
comtd1	C15:6.69	sall1a	C05:21.38	mpx	C16:8.15
C9-like	C16:15.60	*itih3-like*	C06:12.65	fbp1-like	C16:15.64
AS-ES-VHSV		endou	C06:14.43	vmo1-like	C16:16.48
muc2-like	C02:14.16	aldh1l1	C06:26.84	serpina10	C17:11.55
Mx-like	C06:18.75	higd1a	C07:8.33	adh1	C17:16.23
agxtb	C07:10.96	tfa	C07:10.90	kcnh4b	C18:14.21
il8-like	C08:11.73	ahsg2	C07:15.57	ddit4	C18:15.51
pyroxd2	C15:8.58	srd5a1	C07:25.96	***col1a1b***	C18:18.98
AS-PD-ES		fgg	C08:6.04	***prmt1***	C19:1.59
hpxb	C01:2.59	serping1	C08:10.86	ighe	C19:9.44
S100P-like	C01:5.12	prf1-like	C09:1.90	dhx58	C19:16.49
fabp10a	C01:15.18	msmb-like	C09:10.20	***leg1.1***	C20:8.84
apoc2	C01:16.83	fabp	C09:18.29	sgk1	C20:10.25
apoc4	C01:16.83	ccl19-like	C09:23.95	tlr5	C20:17.02
apoa1-like	C01:16.85	gstt1a	C09:24.95	cyp2k1-like	C20:18.76
try2-like	C01:16.92	cpa1-like	C10:2.44	ctl-like	C22:10.60
try1	C01:16.92	myo9Ab-like	C10:6.59	f11-like	C22:12.91

Original studies: AS (Millán et al., 2011; Librán-Pérez et al., 2022); PD (Pardo et al., 2012); VHSV (Díaz-Rosales et al., 2012), ES (Ronza et al., 2016; Robledo et al., 2014).

Gene descriptions: *ctrl1-like* (chymotrypsin-like protease CTRL-1), *rtp3-like* (receptor-transporting protein 3-like), *comtd1* (catechol *O*-methyltransferase domain-containing protein 1), *muc2-like* (mucin-2-like), *agxtb* (alanine-glyoxylate and serine-pyruvate aminotransferase b), *il8-like* (interleukin-8-like), *pyroxd2* (pyridine nucleotide-disulfide oxidoreductase domain-containing protein 2), *hpxb* (hemopexin), *S100P-like* (protein S100-P-like), *fabp10a* (fatty acid-binding protein 10-A), *apoc2* (apolipoprotein C-II), *apoc4* (apolipoprotein C-IV), *apoa1-like* (apolipoprotein A-I-like), *try2-like* (trypsin-2-like), *try1* (trypsin-1), *itih2* (inter-alpha-trypsin inhibitor heavy chain H2), *slc7a1-like* (high affinity cationic amino acid transporter 1-like), *vtnb* (vitronectin b), *mmp13-like* (collagenase 3-like), *ctrb-like* (chymotrypsin B-like), *hp* (haptoglobin), *sall1a* (sal-like protein 1a), *itih3-like* (inter-alpha-trypsin inhibitor heavy chain H3-like), *endou* (poly(U)-specific endoribonuclease-A), *aldh1l1* (cytosolic 10-formyltetrahydrofolate dehydrogenase), *higd1a* (HIG1 domain family member 1A), *tfa* (transferrin-a), *ahsg2* (alpha-2-HS-glycoprotein 2), *srd5a1* (3-oxo-5-alpha-steroid 4-dehydrogenase 1), *msmb-like* (beta-microseminoprotein-like), *fabp* (fatty acid-binding protein, liver-type-like), *gstt1a* (glutathione S-transferase theta-1a), *cpa1-like* (carboxypeptidase A1-like), *myo9Ab-like* (unconventional myosin-IXAb-like), *serpinc1* (antithrombin-III), *fetub* (fetuin-B), *cp* (ceruloplasmin), *agxta* (alanine-glyoxylate and serine-pyruvate aminotransferase a), *dusp1* (dual specificity protein phosphatase 1), *slc40a1* (solute carrier family 40 member 1), *etv5a* (ETS translocation variant 5a), *habp2-like* (hyaluronan-binding protein 2-like), *mpx* (eosinophil peroxidase), *fbp1-like* (fructose-1,6-bisphosphatase 1-like), *vmo1-like* (vitelline membrane outer layer protein 1-like), *serpina10* (protein *Z*-dependent protease inhibitor), *adh1* (alcohol dehydrogenase 1), *kcnh4b* (potassium voltage-gated channel subfamily H member 4), *ddit4* (DNA damage-inducible transcript 4 protein), *col1a1b* (collagen type I alpha 1b), *prmt1* (protein arginine *N*-methyltransferase 1), *ighe* (immunoglobulin epsilon heavy chain), *dhx58* (probable ATP-dependent RNA helicase DHX58), *leg1.1* (liver-enriched gene 1, tandem duplicate 1.

Table 2B
Selection of the most relevant shared tissue specific differentially expressed genes (DEG) across infections with *Aeromonas salmonicida* (AS), *Philasterides dicentrarchi* (PD), *Enteromyxum scophthalmi* (ES) and the VHS virus in *S. maximus*. DEG shared by at least three of the pathogens in spleen and head kidney are shown, with their start position (in Mb) in the respective chromosome (C). In bold, newly annotated genes; underlined nearby genes to the oligos of DEG in the microarray analysis.*

Gene	Position (Mb)	Gene	Position (Mb)	Gene	Position (Mb)
Liver AS-PD		Liver AS-PD (cont)		Spleen AS-PD-ES	
s100p-like	C01:5.12	sgk1	C20:10.25	hpxb	C01:2.59
apoa1-like	C01:16.85	fdft1	C20:11.30	hamp	C01:14.42
ctrl1-like	C01:22.39	pdia4	C21:5.02	fabp10a	C01:15.18
mamu-DRA-like	C02:3.25	fabp3	C22:9.72	***apoc4***	C01:16.83
sult4a1	C02:13.51	ccn4a	C22:10.38	fga-like	C02:1.11
slc7a1-like	C03:8.28	**Head kidney AS-PD-ES-VHSV**		itih2	C02:22.83
hpgd-like	C04:10.20	hamp	C01:14.42	f9b	C04:6.77
sall1a	C05:21.38	**Head kidney AS-PD-VHSV**		mmp13-like	C04:18.93
manf	C06:4.43	aat-like	C20:6.55	hp	C05:10.80
gpd1b	C06:7.35	**Head kidney AS-PD-ES**		aldh1l1	C06:26.84
higd1a	C07:8.33	try2-like	C01:16.92	tfa	C07:10.90
igfbp1	C07:9.75	try1	C01:16.92	ahsg2	C07:15.57
srd5a1	C07:25.96	hp	C05:10.80	serping1	C08:10.86
ho-like	C08:13.18	isp2-like	C05:18.86	C3-like	C08:17.05
isg15	C09:13.88	ccl19-like	C09:23.95	fabp	C09:18.29
fabp	C09:18.29	myo9Ab-like	C10:6.59	serpinc1	C12:0.43
gstt1a	C09:24.95	dusp1	C13:15.38	***fetub***	C12:2.83
hsp90b1	C10:10.35	***col1a1b***	C18:18.98	cp	C12:4.64
pla2-like	C16:4.34	**Head kidney AS-ES-VHSV**		habp2-like	C15:13.68
col1a1b	C18:18.98	Mx-like	C06:18.75	zpi	C17:11.55
prmt1	C19:1.59	il8-like	C08:11.73	adh1	C17:16.23
ighe	C19:9.44	C3-like	C08:17.05	kcnh4b	C18:14.21
gals3a-like	C19:12.74			aat-like	C20:6.55
dhx58	C19:16.49			cyp2k1-like	C20:18.76
leg1.1	C20:8.84			f11-like	C22:12.91

Gene descriptions: mamu-DRA-like (mamu class II histocompatibility antigen, DR alpha chain-like), sult4a1 (sulfotransferase 4A1), hpgd-like (15-hydroxyprostaglandin dehydrogenase [NAD(+)]), manf (mesencephalic astrocyte-derived neurotrophic factor), gpd1b (glycerol-3-phosphate dehydrogenase 1b), igfbp1 (insulin-like growth factor-binding protein 1), ho-like (heme oxygenase-like), isg15 (ubiquitin-like protein ISG15), hsp90b1 (endoplasmin), pla2-like (phospholipase A2, minor isoenzyme-like), gals3a-like (galectin-3-binding protein A-like), fdft1 (squalene synthase), pdia4 (protein disulfide-isomerase A4), fabp3 (fatty acid-binding protein), ccn4a (cellular communication network factor 4a), zpi (protein Z-dependent protease inhibitor).

* Original studies: AS (Millán et al., 2011; Librán-Pérez et al., 2022); PD (Pardo et al., 2012); VHSV (Díaz-Rosales et al., 2012), ES (Ronza et al., 2016; Robledo et al., 2014).

2021). This allowed the annotation of previously unannotated DEG involved in the immune response and the integration of all updated information to identify shared and specific DEG against these pathogens. In addition, QTL data for resistance to the same pathogens (Martínez et al., 2009; Rodríguez-Ramilo et al., 2011, 2013, 2014; Saura et al., 2019), growth (Sánchez-Molano et al., 2011; Sciara et al., 2018) and sex determination (Martínez et al., 2009, 2021; Taboada et al., 2014), as well as outlier loci associated with balancing / divergent (B/D) and domestic / artificial (D/A) selection (do Prado et al., 2018a, 2018b), and

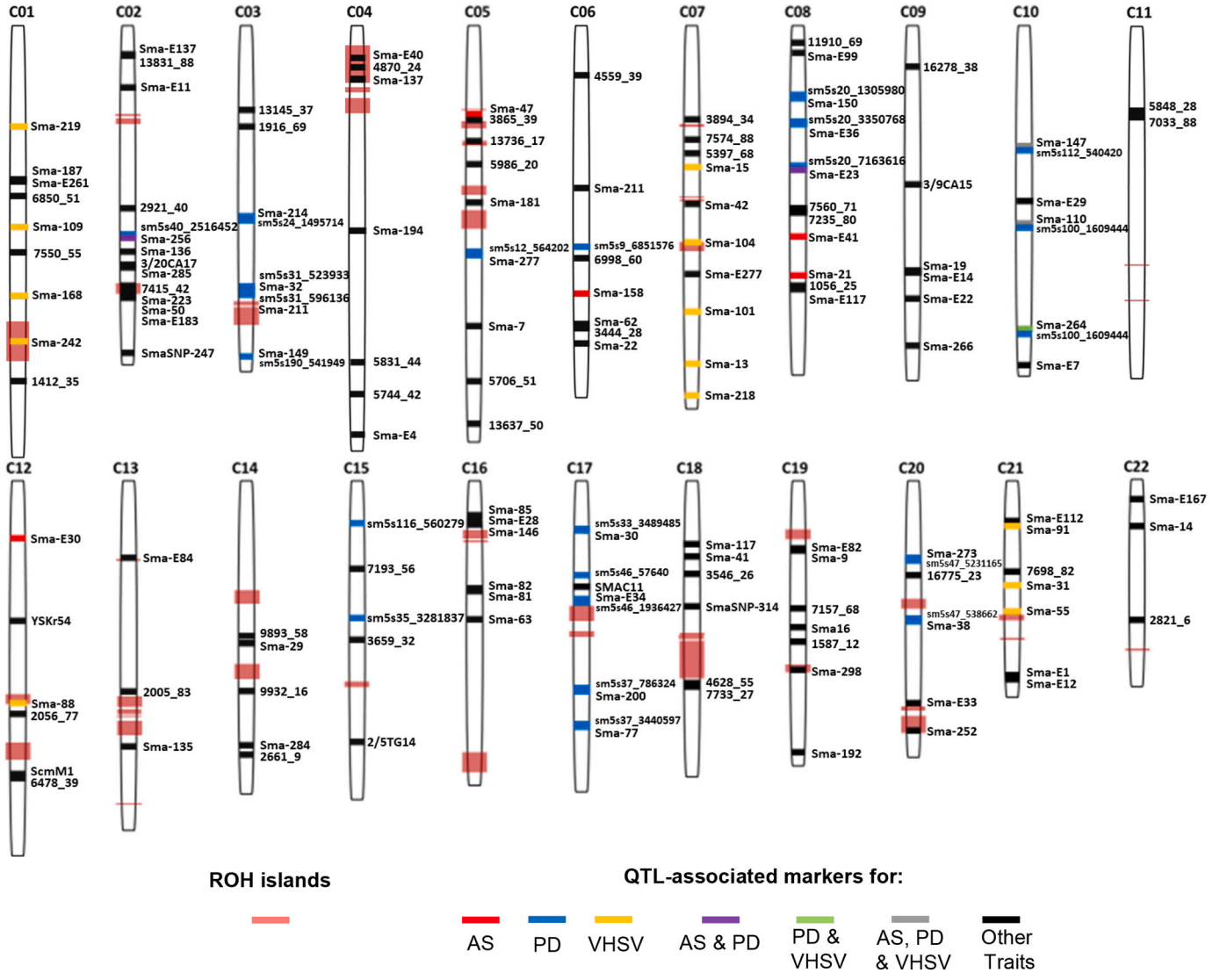

Fig. 4. Position of ROHi (pink) and QTL-associated markers for: resistance to *A. salmonicida* (AS; red), *P. dicentrarchi* (PD; blue), VHSV (yellow), AS & PD (purple), PD & VHSV (green) and AS & PD &VHSV (gray) in *Scophthalmus maximus*. In black, QTL associated markers for all other traits (sex determination, growth, outliers for domestication, balancing and divergent selection). (For interpretation of the references to colour in this figure legend, the reader is referred to the web version of this article.)

runs of homocigosity islands (ROHi; Aramburu et al., 2020) were also integrated as structural landmarks.

Efforts to integrate genomic data generated by the evolving genomic technologies throughout many years are complex due to the different procedures and analytic steps used in each case, and to the progressive enrichment and improvement of public databases (Shen et al., 2014; Liu et al., 2021). Particularly, transcriptomics has experienced a quick evolution in the last decade (Lowe et al., 2017), from the oligo-microarray technology, based on hybridization of a nucleic acid sample to designed oligo-probes (Relógio, 2002), to RNA-seq, which enables the obtention of transcriptome profiles and overcomes some of the limitations of microarrays, such as the requirement of prior knowledge of gene sequences and low accuracy within gene families, paralogous genes and alternative splice variants (Wang et al., 2009).

High quality genome assemblies represent an essential support for updating gene annotation to apply different transcriptomic tools for functional genomic studies in livestock (Hotaling et al., 2021). The progressive improvement on the assembly of genomes is aiding to refine physical mapping and functional annotation for many genes and transcripts, and to discover new genes and functions (Milchevskaya et al., 2017). Localization and annotation of outdated microarray probe information is recommended using up-to-date genomic and transcriptomic resources to facilitate gene expression metadata evaluations (Hadlich et al., 2021). Updating RNA-Seq analyses is also advisable when initial assemblies and preliminary annotations are not stable and undergo successive revisions (Roberts et al., 2013), usual in non-model species and under-represented organisms in genomic databases (Hotaling et al., 2021).

Three out of the six transcriptomic analyses integrated in this study were carried out with an 8x15K Agilent oligo-microarray technology (2716 probes; five technical replicates/gene; Millán et al., 2010) using intraperitoneal challenges of AS (Millán et al., 2011), PD (Pardo et al., 2012) and VHSV (Díaz-Rosales et al., 2012) in turbot. The other three transcriptomic analysis to study early (Ronza et al., 2016) and severe (Robledo et al., 2014) infection by ES, and AS infection (Librán-Pérez et al., 2022) were carried out through oral-challenges(the usual infection route of this gut parasite) and intraperitoneal injection, respectively, using RNA-seq. The differences between these two types of datasets require specific approaches to align transcript oligo-probes or sequences to the current turbot genome and apply appropriate quality

Table 3
Selected differentially expressed genes (DEG) and their association with QTL-associated markers and/or ROH islands (ROHi).

Gene	Position	Function	Marker/ rohi	Category*
celsr1a	C02:15.33	Cell adherence	Sma-256 (AS)	AS-DEG-QTL
dnaja1	C08:9.79	Protein folding	SmaUSC-E23	AS-DEG-QTL
pld5	C08:18.23	T-cell signaling & activation	Sma-USC21	AS-DEG-QTL
CFH-like	C12:3.79	Complement regulation (alt pathway)	Sma-E30 (AS)	AS-DEG-QTL
pdia2	C08:6.26	Protein folding	Sma-E36 (PD)	PD-DEG-QTL
fgg	C08:6.04	Coagulation	Sma-E36 (PD)	PD-DEG-QTL
sgk1	C20:10.25	Inflammatory response	Sma-38 (PD)	PD-DEG-QTL Sh (AS, PD, ES)
hamp	C01:14.42	Iron homeostasis	Sma-109 (VHSV)	VHSV-DEG-QTL Sh (AS, PD, ES, VHSV)
rpl21	C21:2.74	Ribosomal subunit	Sma-91 (VHSV)	VHSV-DEG-QTL
c1qtnf9	C21:2.86	C1q and TNF related	Sma-91 (VHSV)	VHSV-DEG-QTL
plcpi-like	C21:2.45	Proteinase inhibitor	Sma-91 (VHSV)	VHSV-DEG-QTL
mcpt1-like	C12:16.50	Matrix degradation	Sma-88 (VHSV) ROHi_22	UN
myb	C20:10.18	Haematopoiesis, B-lineage development	Sma-38 (PD)	UN
serping1	C08:10.86	C1 inhibitor, complement cascade	Sma-E23 (AS, PD) s20_7163616 (PD)	UN
plg	C20:18.15	Inflammatory response	ROHi_46	Sh (AS, PD, ES, VHSV)
fga-like	C02:1.11	Inflammatory response	Sma-E137 (G) 1381_88 (ID)	Sh (AS, PD, ES, VHSV)
ccl19-like	C09:23.95	Inflammation and homeostasis	Sma-266 (G)	Sh-kidney (AS, PD, ES)
cyp2k1-like	C20:18.76	Inflammatory response	Sma-252 (G) ROHi_46	Sh-Spleen (AS, PD, ES)
kcnh4b	C18:14.21	potassium voltage-gated channel	ROHi_41	Sh-Spleen (AS, PD, ES)
fabp-like	C09:18.29	fatty acid binding protein	Sma-E14 (G) Sma-19 (BS)	Sh-Spleen (AS, PD, ES) Sh-Liver (AS, PD)
ctrl1-like	C01:22.39	chymotrypsin and elastase-like activity	ROHi_01	Sh-Liver (AS, PD)
higd1a	C07:8.33	Inflammatory response	7574_88 (DS)	Sh-Liver (AS, PD)
ho-like	C08:13.18	Heme group degradation	7235_80 (ID) 7560_71 (ID)	Sh-Liver (AS, PD)

* DEG-QTL: Differentially expressed genes near QTL-associated markers for resistance to the same pathogen (*Aeromonas salmonicida* (AS), *Philasterides dicentrarchi* (PD) and VHS virus (VHSV)); Sh: DEG shared in response to different pathogens shown in brackets (AS, PD, VHSV or *Enteromyxum scophthalmi* (ES)), sometimes tissue-specific (kidney, spleen, liver); UN: DEG found around underexplored regions/markers in previous articles (Figueras et al., 2016; Saura et al., 2019; Aramburu et al., 2020).

control measures on the generated data. Oligo-probe sequences of ~50 bp are better aligned using specific software for short DNA sequence reads, like Bowtie 1.3.0. (Langmead et al., 2009), while RNAseq sequences of varying length, from a few hundred bp to thousands, can be better aligned with ncbi-BLAST 2.11 (Morgulis et al., 2008).

A large set of DEG in response to pathogens from the aforementioned studies were integrated into the updated turbot genome assembly harnessing its updated transcriptomic resources (Martínez et al., 2021). Differences in methodological approaches, including the sensitivity and specificity of transcriptomic technologies, the pathogen-specific infective routes and host populations determined unequal number of DEG among studies to be considered for the integration of data. Nevertheless, a quite similar proportion of single-gene hits was obtained across pathogens (78.1%), although lower from microarray (72.9%) than from RNAseq (81.2%) data, as expected given the support for RNAseq analysis of the first turbot genome assembly (Figueras et al., 2016), unavailable when the previous microarray-based studies were developed.

Regarding the annotation success, the datasets coming from microarrays (AS, PD and VHSV) and RNAseq (AS, early and severe ES) showed similar ratios of "conserved", "new" and "lost" annotations, although a striking difference was detected between ES stages for "new" annotations and both studies on AS infection. The presence of newly annotated DEG can be attributed to the improvement of genome assemblies and the progressive refinement and enrichment of functional databases. Specifically in turbot, from the firsts (Figueras et al., 2016; Maroso et al., 2018; Ensembl 103) to the last highly continuous genome version (Martínez et al., 2021; Ensembl 105), a total of 22,751, 21,000 and 21,263 coding genes were annotated respectively, suggesting that the localization and refined annotation of genes and transcripts in the last reference genome are more relevant than the number of genes itself to account for the results observed.

Genomic analysis greatly benefits from studies where generated data is easily available, opening the possibilities for comparison between diseases involving the same or different pathogens. This allowed us to compare two distinct DEG datasets in response to AS in head kidney 24 hpi (Millán et al., 2011; Librán-Pérez et al., 2022), which unveiled a total of 15 shared DEG, some of them involved in the complement system (*c3-like*, *c4b* (complement C4—B)), IFN pathway (*Mx-like* (interferon-induced GTP-binding protein Mx-like)), chemokines (*ccl19-like* (C—C motif chemokine 19-like)) or antimicrobial response (*hamp*), proving the robustness of these independent findings.

Other studies have provided interesting information on the turbot transcriptome response to VHSV (Pereiro et al., 2014) and PD (Valle et al., 2020) infections with microarray and RNAseq technology, respectively, but they could not be included in our bioinformatic analysis because the sequences for the identified DEGs are not available. In any case, qualitative comparisons could be made for the same diseases using the DEG annotations from these studies and the annotation recorded in our work, revealing that some key gene families involved in acute response were being regulated: the complement system (*C1qtnf9*, *C3-like*, *C8g* (complement component C8 gamma chain), *C9-like* (complement component C9-like)) was found to be regulated for both pathogens in either of the four studies (Diaz-Rosales et al. 2012; Pardo et al., 2012; Pereiro et al., 2014; Valle et al., 2020), while other pathways were particularly conserved between studies for the same pathogen, such as the IFN signaling pathway (*mx-like*, *Ifi27l2a* (interferon alpha-inducible protein 27-like protein 2A)), coagulation proteins (*col4a6* (collagen alpha-6(IV) chain), *fga-like*, *plg*) and pro-inflammatory genes (*hamp*, *ndfip2* (NEDD4 family-interacting protein 2), muc2-like (mucin-2-like), lgals9-like (galectin-9-like), *gp1bb* (platelet glycoprotein Ib beta chain)) for both VHSV studies (Pardo et al., 2012; Valle et al., 2020), and immunoglobulins (*iglc1-like*(immunoglobulin lambda-1 light chain-like)), perforins (*prf1-like* (perforin-1-like)), chemokines (*ccl19-like*, *cxcl14* (C-X-C motif chemokine 14)) and toll-like receptors (*tlr5* (toll-like receptor 5)) for both PD studies.

All trait-associated markers and ROHi were repositioned successfully in the updated turbot assembly, albeit three ROHi among 49 showed remarkable size differences between the original study and this atlas. The scaffolds used for ROHi analysis came from the first rather fragmented and slightly incomplete turbot genome version (N50: 4.3 Mb, 287 scaffolds >166 kb covering 95% of the total genome size, 544 Mb; Figueras et al., 2016) respect to the updated assembly (N50: 22.9 Mb, 27 contigs covering 95% of the total genome, 560 Mb; Martínez et al., 2021). Despite this new genome showed a high correspondence with the previous version using a highly dense genetic map (Maroso et al., 2018),

important discrepancies were found at telomeric and centromeric regions (Martínez et al., 2021). Indeed, the three discrepant ROHi spanned regions included in short scaffolds anchored near telomeric regions, suggesting assembly problems due to repetitive DNA. Even so, ROHi data were mostly confirmed, supporting gene mining underlying putative selective sweeps related to disease resistance and other productive traits (Aramburu et al., 2020).

The updated integrative map presented can be used to identify candidate genes underlying resistance to pathologies through exploring DEG near QTL-associated markers for resistance to the same pathogens. Some genes were unveiled, such as *celsr1a, dnaja1 and apoh-like* (AS); *fgg, pdia2* and *sgk1* (PD), or *c1qtnf9* and *hamp* (VHSV), with important immune functions and related to diseases in other domestic species (Li et al., 2020; Kotlarz et al., 2013; Zhu et al., 2018; Sun et al., 2022; Stolf et al., 2011; Zhu et al., 2015; Xu et al., 2019; Rodrigues et al., 2006).

The atlas can also be helpful for reanalysing poorly characterized regions from previous studies (Figueras et al., 2016; Aramburu et al., 2020). For instance, *mcpt1-like* (mast cell protease 1A-like), a gene involved in general infective processes, related to viral and bacterial infection immunity (St John et al., 2013; Piliponsky et al., 2019), was detected close to the VHSV-associated marker Sma-USC88. Also, *myb* (v-myb avian myeloblastosis viral oncogene homolog), crucial for normal haematopoiesis and B-lineage development (Fahl et al., 2009), and *sgk1*, a key regulator of neutrophil clearance during inflammation resolution in zebrafish (Burgon et al., 2014) were detected near the PD-associated marker Sma-USC38. Crossing functional information with other genetic evaluation layers can provide more consistent candidate genes, and for example, the outlined Sma-USC88 marker was detected inside ROHi-22, suggesting being involved in D/A selection in turbot farms.

One of the key outcomes of this integrative study was the unveiling of shared DEG across the different infective diseases. Among the six DEG regulated in all the four diseases, *hamp*, *plg* and *fga-like* were of particular interest since they were found within/near significant structural genomic features, such as ROHi, QTL or outlier markers. *Hamp,* as previously remarked by Millán et al., 2011, Pardo et al., 2012) and Robledo et al. (2014), is involved in iron homeostasis and resistance to bacterial infection and was up-regulated in head kidney in three of the pathogens studied, except for VHSV (down-regulated). It was also up-regulated in spleen after AS, PD and ES challenges. Furthermore, this gene has been reported to be involved in resistance to bacterial infection (Rodrigues et al., 2006) and used for treatment against bacterial infections and iron disorders (Barroso et al., 2021) in *Dicentrarchus labrax*. *Plg* is a key activator of the inflammatory response, which facilitates leukocyte recruitment in the site of infection, as well as coagulation, and has been reported in response against *Paramoeba perurans* in *Atlantic salmon* (McCormack et al., 2021). *Plg* was differentially expressed in head kidney during ES severe infection (up-regulated) and VHSV (down-regulated) and in spleen by AS (mostly down-regulated) and PD (up-regulated early to mid-infection), pointing to distinct expression profiles for candidate genes across pathogens. Its location inside a ROHi and its immune relevance across all four infections suggest that it could be a target of selective breeding programs, focused on growth and/or immune-related genes (López et al., 2019). Involved in similar functions as *plg* is the *fga-like* gene, which was also found to be modulated in the four infective responses: in head kidney after PD challenge (up-regulated, late infection) and VHSV (down-regulated, all time around); and in spleen after AS challenge (up-regulated, mid-infection), PD (up-regulated early-mid infection) and ES (down-regulated, early stages). Its importance at early stages of pathogen-specific infection due to triggering the inflammatory response was remarked previously (Millán et al., 2011; Pardo et al., 2012; Díaz-Rosales et al., 2012). Both *plg* and *fga-like* participate in the coagulation cascade, that has been identified as a key mechanism in the defence against PD (Blanco-Abad et al., 2018), and mapped close to ROHi (ROHi_46) and QTL markers (Sma-E137 and 13831_88), respectively. Interestingly, the fibrinogen coding gene was downregulated in low mortality families in response to VHSV, suggesting that overexpression of this gene could facilitate opportunistic bacterial infections. During infections, both specific and shared responses to pathogens are triggered, involving different defence and immune genes (Goncalves et al., 2014). Exploration of the complex responses across pathogens through integrative genomics allows to revise and identify new biomarkers for diseases caused by different types of bacteria, viruses, and parasites (Natnan et al., 2021).

Going beyond the gene level analysis is essential in functional genomic studies trying to integrate the DEG into common pathways or functions over or underrepresented with regard to the appropriate transcriptomic background. In general, most of the enriched GO terms detected in response to AS, PD and ES belong to one or more of the categories described in the original studies, suggesting a general conservation of the functional profiles previously reported (Millan et al., 2011; Pardo et al., 2012, Robledo et al., 2014, Ronza et al., 2016, Librán-Pérez et al., 2022). In the case of VHSV resistance, the low number of DEG studied explains the presence of only 20 significant GO terms, all associated to metabolic process and transport. Interestingly, some GO terms were associated with organ morphogenesis and neurogenesis, which also appeared in the functional enrichment of early and late enteromyxosis, unreported in the original studies (Robledo et al., 2014; Ronza et al., 2016). In gastrointestinal infections, alteration of the enteric nervous system needs to be considered, as parasitic infections have been found to alter the enteric nervous system *via* nerve distribution, neurochemical levels and neuronal functions (Halliez and Buret, 2015).

5. Conclusions

In this work, an atlas of functional genomic elements related to disease response in turbot has been generated through integrating published information on the updated turbot assembly, which unveiled shared and disease-specific differentially expressed genes for four key infective diseases. The functional elements identified in this atlas could constitute useful biomarkers for improving breeding programs in turbot, since functional annotation (and more recently, regulatory data) is crucial for understanding the molecular mechanisms underlying complex commercial traits. Similar studies are being developed in turbot in the framework of the AQUAFAANG project (Clark et al., 2020), where atlases for regulatory elements are being characterized across development, tissues, and life stages, which can aid to increase precision in genomic breeding values.

Supplementary data to this article can be found online at https://doi.org/10.1016/j.aquaculture.2022.739067.

Funding

This work was supported by the European Union's Horizon 2020 research and innovation programme (Grant number No 817923), and the Regional Government Xunta de Galicia (Spain) (Consolidation and Structuring of competitive research units, ED431C 2022/33). OA was supported by a predoctoral research fellowship from Xunta de Galicia (Grant number ED481A2020/119).

CRediT authorship contribution statement

Oscar Aramburu: Investigation, Formal analysis, Writing – original draft, Writing – review & editing. **Andrés Blanco:** Investigation, Formal analysis. **Carmen Bouza:** Conceptualization, Supervision, Investigation, Formal analysis, Writing – original draft, Writing – review & editing. **Paulino Martínez:** Conceptualization, Supervision, Funding acquisition, Investigation, Formal analysis, Writing – original draft, Writing – review & editing.

Declaration of Competing Interest

The authors declare that they have no known competing financial interests or personal relationships that could have appeared to influence the work reported in this paper.

Data availability

Our research data will be made available as supplementary material.

Acknowledgements

The work presented in this manuscript was made possible due to computational support for the bioinformatic analysis provided by Centro de Supercomputación de Galicia (CESGA).

References

APROMAR, 2021. Informe 2021: La Acuicultura en España. Spanish gobernment. apromar.es.

Aramburu, O., Ceballos, F., Casanova, A., le Moan, A., Hemmer-Hansen, J., Bekkevold, D., Bouza, C., Martínez, P., 2020. Genomic signatures after five generations of intensive selective breeding: runs of homozygosity and genetic diversity in representative domestic and wild populations of turbot (Scophthalmus maximus). Front. Genet. 11 https://doi.org/10.3389/fgene.2020.00296.

Barroso, C., Carvalho, P., Nunes, M., Gonçalves, J., Rodrigues, P., Neves, J., 2021. The era of antimicrobial peptides: use of hepcidins to prevent or treat bacterial infections and Iron disorders. Front. Immunol. 12 https://doi.org/10.3389/fimmu.2021.754437.

Blanco-Abad, V., Noia, M., Valle, A., Fontenla, F., Folgueira, I., De Felipe, A.P., Pereiro, P., Leiro, J., Lamas, J., 2018. The coagulation system helps control infection caused by the ciliate parasite Philasterides dicentrarchi in the turbot Scophthalmus maximus (L.). Dev. Comp. Immunol. 87, 147–156. https://doi.org/10.1016/j.dci.2018.06.001.

Budiño, B., Pata, M.P., Leiro, J., Lamas, J., 2012. Differences in the in vitro susceptibility to resveratrol and other chemical compounds among several Philasterides dicentrarchi isolates from turbot. Parasitol. Res. 110 (4), 1573–1578. https://doi.org/10.1007/s00436-011-2664-1.

Burgon, J., Robertson, A.L., Sadiku, P., Wang, X., Hooper-Greenhill, E., Prince, L.R., Walker, P., Hoggett, E.E., Ward, J.R., Farrow, S.N., Zuercher, W.J., Jeffrey, P., Savage, C.O., Ingham, P.W., Hurlstone, A.F., Whyte, M.K.B., Renshaw, S.A., 2014. Serum and glucocorticoid–regulated kinase 1 regulates neutrophil clearance during inflammation resolution. J. Immunol. 192 (4), 1796–1805. https://doi.org/10.4049/jimmunol.1300087.

Clark, E.L., Archibald, A.L., Daetwyler, H.D., Groenen, M.A.M., Harrison, P.W., Houston, R.D., Kühn, C., Lien, S., Macqueen, D.J., Reecy, J.M., Robledo, D., Watson, M., Tuggle, C.K., Giuffra, E., 2020. From FAANG to fork: application of highly annotated genomes to improve farmed animal production. Genome Biol. 21 (1), 285. https://doi.org/10.1186/s13059-020-02197-8.

Díaz-Rosales, P., Romero, A., Balseiro, P., Dios, S., Novoa, B., Figueras, A., 2012. Microarray-based identification of differentially expressed genes in families of turbot (Scophthalmus maximus) after infection with viral haemorrhagic septicaemia virus (VHSV). Mar. Biotechnol. 14 (5), 515–529. https://doi.org/10.1007/s10126-012-9465-0.

do Prado, F.D., Vera, M., Hermida, M., Bouza, C., Pardo, B.G., Vilas, R., Blanco, A., Fernández, C., Maroso, F., Maes, G.E., Turan, C., Volckaert, F.A.M., Taggart, J.B., Carr, A., Ogden, R., Nielsen, E.E., Martínez, P., 2018a. Parallel evolution and adaptation to environmental factors in a marine flatfish: implications for fisheries and aquaculture management of the turbot (Scophthalmus maximus). Evol. Appl. 11 (8), 1322–1341. https://doi.org/10.1111/eva.12628.

do Prado, F., Vera, M., Hermida, M., Blanco, A., Bouza, C., Maes, G., Volckaert, F., Aquatrace, C., Martínez, P., 2018b. Tracing the genetic impact of farmed turbot Scophthalmus maximus on wild populations. Aquac. Environ. Interactions 10, 447–463. https://doi.org/10.3354/aei00282.

Elaswad, A., Dunham, R., 2018. Disease reduction in aquaculture with genetic and genomic technology: current and future approaches. Rev. Aquac. 10 (4), 876–898. https://doi.org/10.1111/raq.12205.

Ellis, A.E., 1997. Immunization with bacterial antigens: furunculosis. Dev. Biol. Stand. 90, 107–116 (PMID: 9270839).

Fahl, S.P., Crittenden, R.B., Allman, D., Bender, T.P., 2009. C-Myb is required for pro-B cell differentiation. J. Immunol. 183 (9), 5582–5592. https://doi.org/10.4049/jimmunol.0901187.

Figueras, A., Robledo, D., Corvelo, A., Hermida, M., Pereiro, P., Rubiolo, J.A., Gómez-Garrido, J., Carreté, L., Bello, X., Gut, M., Gut, I.G., Marcet-Houben, M., Forn-Cuní, G., Galán, B., García, J.L., Abal-Fabeiro, J.L., Pardo, B.G., Taboada, X., Fernández, C., Martínez, P., 2016. Whole genome sequencing of turbot (*Scophthalmus maximus* ; Pleuronectiformes): a fish adapted to demersal life. DNA Res. 23 (3), 181–192. https://doi.org/10.1093/dnares/dsw007.

Fraslin, C., Quillet, E., Rochat, T., Dechamp, N., Bernardet, J.-F., Collet, B., Lallias, D., Boudinot, P., 2020. Combining multiple approaches and models to dissect the genetic architecture of resistance to infections in fish. Front. Genet. 11 https://doi.org/10.3389/fgene.2020.00677.

Garcia, B.F., Bonaguro, Á., Araya, C., Carvalheiro, R., Yáñez, J.M., 2021. Application of a novel 50K SNP genotyping array to assess the genetic diversity and linkage disequilibrium in a farmed Pacific white shrimp (Litopenaeus vannamei) population. Aquac. Rep. 20, 100691 https://doi.org/10.1016/j.aqrep.2021.100691.

Ge, S.X., Jung, D., Yao, R., 2020. ShinyGO: a graphical gene-set enrichment tool for animals and plants. Bioinformatics 36 (8), 2628–2629. https://doi.org/10.1093/bioinformatics/btz931.

Gjedrem, T., Rye, M., 2018. Selection response in fish and shellfish: a review. Rev. Aquac. 10 (1), 168–179. https://doi.org/10.1111/raq.12154.

Goncalves, P., Guertler, C., Bachère, E., de Souza, C.R.B., Rosa, R.D., Perazzolo, L.M., 2014. Molecular signatures at imminent death: hemocyte gene expression profiling of shrimp succumbing to viral and fungal infections. Dev. Comp. Immunol. 42 (2), 294–301. https://doi.org/10.1016/j.dci.2013.09.017.

Gutierrez, A.P., Bean, T.P., Hooper, C., Stenton, C.A., Sanders, M.B., Paley, R.K., Rastas, P., Bryrom, M., Matika, O., Houston, R.D., 2018. A genome-wide association study for host resistance to ostreid herpesvirus in Pacific oysters (Crassostrea gigas). G3: Genes Genomes Gene. 8 (4), 1273–1280. https://doi.org/10.1534/g3.118.200113.

Hadlich, F., Reyer, H., Oster, M., Trakooljul, N., Murani, E., Ponsuksili, S., Wimmers, K., 2021. rePROBE: workflow for revised probe assignment and updated probe-set annotation in microarrays. Genomics Proteomics Bioinforma. https://doi.org/10.1016/j.gpb.2020.06.007.

Halliez, M.C.M., Buret, A.G., 2015. Gastrointestinal parasites and the neural control of Gut functions. Front. Cell. Neurosci. 9 https://doi.org/10.3389/fncel.2015.00452.

Hotaling, S., Kelley, J.L., Frandsen, P.B., 2021. Toward a genome sequence for every animal: where are we now? Proc. Natl. Acad. Sci. 118 (52) https://doi.org/10.1073/pnas.2109019118.

Houston, R.D., Bean, T.P., Macqueen, D.J., Gundappa, M.K., Jin, Y.H., Jenkins, T.L., Selly, S.L.C., Martin, S.A.M., Stevens, J.R., Santos, E.M., Davie, A., Robledo, D., 2020. Harnessing genomics to fast-track genetic improvement in aquaculture. Nat. Rev. Genet. 21 (7), 389–409. https://doi.org/10.1038/s41576-020-0227-y.

Iglesias, R., Paramá, A., Alvarez, M., Leiro, J., Fernández, J., Sanmartín, M., 2001. Philasterides dicentrarchi (Ciliophora, Scuticociliatida) as the causative agent of scuticociliatosis in farmed turbot Scophthalmus maximus in Galicia (NW Spain). Dis. Aquat. Org. 46, 47–55. https://doi.org/10.3354/dao046047.

Knap, P.W., Doeschl-Wilson, A., 2020. Why breed disease-resilient livestock, and how? Genet. Sel. Evol. 52 (1), 60. https://doi.org/10.1186/s12711-020-00580-4.

Kotlarz, A., Tukaj, S., Krzewski, K., Brycka, E., Lipinska, B., 2013. Human Hsp40 proteins, DNAJA1 and DNAJA2, as potential targets of the immune response triggered by bacterial DnaJ in rheumatoid arthritis. Cell Stress Chaperones 18 (5), 653–659. https://doi.org/10.1007/s12192-013-0407-1.

Langmead, B., Trapnell, C., Pop, M., Salzberg, S.L., 2009. Ultrafast and memory-efficient alignment of short DNA sequences to the human genome. Genome Biol. 10 (3), R25. https://doi.org/10.1186/gb-2009-10-3-r25.

León-Rodríguez, L., Luzardo-Álvarez, A., Blanco-Méndez, J., Lamas, J., Leiro, J., 2012. A vaccine based on biodegradable microspheres induces protective immunity against scuticociliatosis without producing side effects in turbot. Fish Shellfish Immunol. 33 (1), 21–27. https://doi.org/10.1016/j.fsi.2012.03.028.

Li, C., Barton, C., Henke, K., Daane, J., Treaster, S., Caetano-Lopes, J., Tanguay, R.L., Harrys, M.P., 2020. Celsr1a is essential for tissue homeostasis and onset of aging phenotypes in the zebrafish. Elife 9. https://doi.org/10.7554/elife.50523.

Librán-Pérez, M., Pereiro, P., Figueras, A., Novoa, B., 2022. Transcriptome analysis of turbot (Scophthalmus maximus) infected with Aeromonas salmonicida reveals a direct effect on leptin synthesis as a neuroendocrine mediator of inflammation and metabolism regulation. Front. Mar. Sci. 9 https://doi.org/10.3389/fmars.2022.888115, 888115.

Liu, F., Li, Y., Yu, H., Zhang, L., Hu, J., Bao, Z., Wang, S., 2021. MolluscDB: an integrated functional and evolutionary genomics database for the hyper-diverse animal phylum Mollusca. Nucleic Acids Res. 49 (D1) https://doi.org/10.1093/nar/gkaa918. D988–D997.

López, M.E., Linderoth, T., Norris, A., Lhorente, J.P., Neira, R., Yáñez, J.M., 2019. Multiple selection signatures in farmed Atlantic Salmon adapted to different environments across hemispheres. Front. Genet. 10 https://doi.org/10.3389/fgene.2019.00901.

Lowe, R., Shirley, N., Bleackley, M., Dolan, S., Shafee, T., 2017. Transcriptomics technologies. PLoS Comput. Biol. 13 (5) https://doi.org/10.1371/journal.pcbi.1005457 e1005457.

Ma, A., Huang, Z., Wang, X., Xu, Y., Guo, X., 2021. Identification of quantitative trait loci associated with upper temperature tolerance in turbot, *Scophthalmus maximus*. Sci. Rep. 11 (1), 21920. https://doi.org/10.1038/s41598-021-01062-3.

Maroso, F., Hermida, M., Millán, A., Blanco, A., Saura, M., Fernández, A., Dalla Rovere, G., Bargelloni, L., Cabaleiro, S., Villanueva, B., Bouza, C., Martínez, P., 2018. Highly dense linkage maps from 31 full-sibling families of turbot (Scophthalmus maximus) provide insights into recombination patterns and chromosome rearrangements throughout a newly refined genome assembly. DNA Res. 25 (4), 439–450. https://doi.org/10.1093/dnares/dsy015.

Martínez, P., 2016. Genomics advances for boosting aquaculture breeding programs in Spain. Aquaculture 464, 117–120. https://doi.org/10.1016/j.aquaculture.2016.06.021.

Martínez, P., Bouza, C., Hermida, M., Fernández, J., Toro, M.A., Vera, M., Pardo, B., Millán, A., Fernández, C., Vilas, R., Viñas, A., Sánchez, L., Felip, A., Piferrer, F., Ferreiro, I., Cabaleiro, S., 2009. Identification of the major sex-determining region of turbot (Scophthalmus maximus). Genetics 183 (4), 1443–1452. https://doi.org/10.1534/genetics.109.107979.

Martínez, P., Robledo, D., Taboada, X., Blanco, A., Moser, M., Maroso, F., Hermida, M., Gómez-Tato, A., Álvarez-Blázquez, B., Cabaleiro, S., Piferrer, F., Bouza, C., Lien, S., Viñas, A.M., 2021. A genome-wide association study, supported by a new chromosome-level genome assembly, suggests sox2 as a main driver of the undifferentiatiated ZZ/ZW sex determination of turbot (Scophthalmus maximus). Genomics 113 (4), 1705–1718. https://doi.org/10.1016/j.ygeno.2021.04.007.

McCormack, M., Talbot, A., Dillon, E., O'Connor, I., MacCarthy, E., 2021. Host response of Atlantic Salmon (Salmo salar) re-inoculated with Paramoeba perurans. Microorganisms 9 (5), 993. https://doi.org/10.3390/microorganisms9050993.

Metzger, J., Karwath, M., Tonda, R., Beltran, S., Águeda, L., Gut, M., et al., 2015. Runs of homozygosity reveal signatures of positive selection for reproduction traits in breed and non-breed horses. BMC Genomics 16, 764. https://doi.org/10.1186/s12864-015-1977-3.

Milchevskaya, V., Tödt, G., Gibson, T.J., 2017. A tool to build up-to-date gene annotations for Affymetrix microarrays. Genomics Comput. Biol. 3 (2), 38. https://doi.org/10.18547/gcb.2017.vol3.iss2.e38.

Millán, A., Gómez-Tato, A., Fernández, C., Pardo, B.G., Álvarez-Dios, J.A., Calaza, M., Bouza, C., Vázquez, M., Cabaleiro, S., Martínez, P., 2010. Design and performance of a turbot (Scophthalmus maximus) oligo-microarray based on ESTs from immune tissues. Mar. Biotechnol. 12 (4), 452–465. https://doi.org/10.1007/s10126-009-9231-0.

Millán, A., Gómez-Tato, A., Pardo, B.G., Fernández, C., Bouza, C., Vera, M., Alvarez-Dios, J.A., Cabaleiro, S., Lamas, J., Lemos, M.L., Martínez, P., 2011. Gene expression profiles of the spleen, liver, and head kidney in turbot (Scophthalmus maximus) along the infection process with Aeromonas salmonicida using an immune-enriched oligo-microarray. Mar. Biotechnol. 13 (6), 1099–1114. https://doi.org/10.1007/s10126-011-9374-7.

Morgulis, A., Coulouris, G., Raytselis, Y., Madden, T.L., Agarwala, R., Schäffer, A.A., 2008. Database indexing for production MegaBLAST searches. Bioinformatics 24 (16), 1757–1764. https://doi.org/10.1093/bioinformatics/btn322.

Munang'andu, H., Galindo-Villegas, J., David, L., 2018. Teleosts genomics: progress and prospects in disease prevention and control. Int. J. Mol. Sci. 19 (4), 1083. https://doi.org/10.3390/ijms19041083.

Natnan, M.E., Low, C.-F., Chong, C.-M., Bunawan, H., Baharum, S.N., 2021. Integration of omics tools for understanding the fish immune response due to microbial challenge. Front. Mar. Sci. 8 https://doi.org/10.3389/fmars.2021.668771.

Ødegård, J., Baranski, M., Gjerde, B., Gjedrem, T., 2011. Methodology for genetic evaluation of disease resistance in aquaculture species: challenges and future prospects. Aquac. Res. 42, 103–114. https://doi.org/10.1111/j.1365-2109.2010.02669.x.

Owens, L., 2012. Chapter 10: Diseases. In: Lucas, J.S., Southgate, P.C. (Eds.), Aquaculture: Farming Aquatic Animals and Plants, Second edition. Blackwell Publishing Ltd., pp. 214–228. https://doi.org/10.1002/9781118687932

Paramá, A., Iglesias, R., Álvarez, M.F., Sanmartín, M.L., Leiro, J., 2004. Chemotactic responses of the fish-parasitic scuticociliate Philasterides dicentrarchi to blood and blood components of the turbot Scophthalmus maximus, evaluated using a new microplate multiassay. J. Microbiol. Methods 58 (3), 361–366. https://doi.org/10.1016/j.mimet.2004.04.018.

Paramá, A., Luzardo, A., Blanco-Méndez, J., Sanmartín, M., Leiro, J., 2005. In vitro efficacy of glutaraldehyde-crosslinked chitosan microspheres against the fish-pathogenic ciliate Philasterides dicentrarchi. Dis. Aquat. Org. 64, 151–158. https://doi.org/10.3354/dao064151.

Pardo, B.G., Millán, A., Gómez-Tato, A., Fernández, C., Bouza, C., Alvarez-Dios, J.A., Cabaleiro, S., Lamas, J., Leiro, J.M., Martínez, P., 2012. Gene expression profiles of spleen, liver, and head kidney in turbot (Scophthalmus maximus) along the infection process with Philasterides dicentrarchi using an immune-enriched oligo-microarray. Mar. Biotechnol. 14 (5), 570–582. https://doi.org/10.1007/s10126-012-9440-9.

Park, K.C., Osborne, J.A., Montes, A., Dios, S., Nerland, A.H., Novoa, B., Figueras, A., Brown, L.L., Johnson, S.C., 2009. Immunological responses of turbot (Psetta maxima) to nodavirus infection or polyriboinosinic polyribocytidylic acid (pIC) stimulation, using expressed sequence tags (ESTs) analysis and cDNA microarrays. Fish Shellfish Immunol. 26 (1), 91–108. https://doi.org/10.1016/j.fsi.2008.03.010.

Peñaloza, C., Manousaki, T., Franch, R., Tsakogiannis, A., Sonesson, A.K., Aslam, M.L., Allal, F., Bargelloni, L., Houston, R.D., Tsigenopoulos, C.S., 2021. Development and testing of a combined species SNP array for the European seabass (Dicentrarchus labrax) and gilthead seabream (Sparus aurata). Genomics 113 (4), 2096–2107. https://doi.org/10.1016/j.ygeno.2021.04.038.

Pereiro, P., Dios, S., Boltaña, S., Coll, J., Estepa, A., Mackenzie, S., et al., 2014. Transcriptome profiles associated to VHSV infection or DNA vaccination in turbot (Scophthalmus maximus). PLoS One 9 (8), e104509. https://doi.org/10.1371/journal.pone.0104509.

Pereiro, P., Figueras, A., Novoa, B., 2016. Turbot (Scophthalmus maximus) vs. VHSV (viral hemorrhagic septicemia virus): a review. Front. Physiol. 7 https://doi.org/10.3389/fphys.2016.00192.

Piliponsky, A.M., Acharya, M., Shubin, N.J., 2019. Mast cells in viral, bacterial, and fungal infection immunity. Int. J. Mol. Sci. 20 (12), 2851. https://doi.org/10.3390/ijms20122851.

Relógio, A., 2002. Optimization of oligonucleotide-based DNA microarrays. Nucleic Acids Res. 30 (11), 51e–551. https://doi.org/10.1093/nar/30.11.e51.

Roberts, A., Schaeffer, L., Pachter, L., 2013. Updating RNA-Seq analyses after re-annotation. Bioinformatics 29 (13), 1631–1637. https://doi.org/10.1093/bioinformatics/btt197.

Robledo, D., Ronza, P., Harrison, P.W., Losada, A.P., Bermúdez, R., Pardo, B.G., José Redondo, M., Sitjà-Bobadilla, A., Quiroga, M.I., Martínez, P., 2014. RNA-seq analysis reveals significant transcriptome changes in turbot (Scophthalmus maximus) suffering severe enteromyxosis. BMC Genomics 15 (1), 1149. https://doi.org/10.1186/1471-2164-15-1149.

Rodrigues, P., Vázquez-Dorado, S., Neves, J., Wilson, J., 2006. Dual function of fish hepcidin: response to experimental iron overload and bacterial infection in sea bass (Dicentrarchus labrax). Dev. Comp. Immunol. 30 (12), 1156–1167. https://doi.org/10.1016/j.dci.2006.02.005.

Rodríguez-Ramilo, S.T., Toro, M.A., Bouza, C., Hermida, M., Pardo, B.G., Cabaleiro, S., Martínez, P., Fernández, J., 2011. QTL detection for Aeromonas salmonicida resistance related traits in turbot (Scophthalmus maximus). BMC Genomics 12 (1), 541. https://doi.org/10.1186/1471-2164-12-541.

Rodríguez-Ramilo, S.T., Fernández, J., Toro, M.A., Bouza, C., Hermida, M., Fernández, C., Pardo, B.G., Cabaleiro, S., Martínez, P., 2013. Uncovering QTL for resistance and survival time to Philasterides dicentrarchi in turbot (Scophthalmus maximus). Anim. Genet. 44 (2), 149–157. https://doi.org/10.1111/j.1365-2052.2012.02385.x.

Rodríguez-Ramilo, S.T., de La Herrán, R., Ruiz-Rejón, C., Hermida, M., Fernández, C., Pereiro, P., Figueras, A., Bouza, C., Toro, M.A., Martínez, P., Fernández, J., 2014. Identification of quantitative trait loci associated with resistance to viral haemorrhagic septicaemia (VHS) in turbot (Scophthalmus maximus): a comparison between bacterium, Parasite and Virus Diseases. Mar. Biotechnol. 16 (3), 265–276. https://doi.org/10.1007/s10126-013-9544-x.

Ronza, P., Robledo, D., Bermúdez, R., Losada, A.P., Pardo, B.G., Sitjà-Bobadilla, A., Quiroga, M.I., Martínez, P., 2016. RNA-seq analysis of early enteromyxosis in turbot (Scophthalmus maximus): new insights into parasite invasion and immune evasion strategies. Int. J. Parasitol. 46 (8), 507–517. https://doi.org/10.1016/j.ijpara.2016.03.007.

Ronza, P., Robledo, D., Bermúdez, R., Losada, A.P., Pardo, B.G., Martínez, P., Quiroga, M.I., 2019. Integrating genomic and morphological approaches in fish pathology research: the case of turbot (Scophthalmus maximus) Enteromyxosis. Front. Genet. 10 https://doi.org/10.3389/fgene.2019.00026.

Sánchez-Molano, E., Cerna, A., Toro, M.A., Bouza, C., Hermida, M., Pardo, B.G., Cabaleiro, S., Fernández, J., Martínez, P., 2011. Detection of growth-related QTL in turbot (Scophthalmus maximus). BMC Genomics 12 (1), 473. https://doi.org/10.1186/1471-2164-12-473.

Saura, M., Carabaño, M.J., Fernández, A., Cabaleiro, S., Doeschl-Wilson, A.B., Anacleto, O., Maroso, F., Millán, A., Hermida, M., Fernández, C., Martínez, P., Villanueva, B., 2019. Disentangling genetic variation for resistance and endurance to Scuticociliatosis in turbot using pedigree and genomic information. Front. Genet. 10 https://doi.org/10.3389/fgene.2019.00539.

Sciara, A.A., Rodríguez-Ramilo, S.T., Hermida, M., Gómez-Tato, A., Fernández, J., Bouza, C., Martínez, P., 2018. Validation of growth-related quantitative trait loci markers in turbot (Scophthalmus maximus) families as a step toward marker assisted selection. Aquaculture 495, 602–610. https://doi.org/10.1016/j.aquaculture.2018.06.010.

Shen, L., Shao, N., Liu, X., Nestler, E., 2014. Ngs.Plot: quick mining and visualization of next-generation sequencing data by integrating genomic databases. BMC Genomics 15 (1), 284. https://doi.org/10.1186/1471-2164-15-284.

St John, A.L., Rathore, A.P., Raghavan, B., Ng, M.-L., Abraham, S.N., 2013. Contributions of mast cells and vasoactive products, leukotrienes and chymase, to dengue virus-induced vascular leakage. ELife 2. https://doi.org/10.7554/eLife.00481.

Stolf, B.S., Smyrnias, I., Lopez, L.R., Vendramin, A., Goto, H., Laurindo, F.R.M., Shah, A. M., Santos, C.X.C., 2011. Sci. World J. 11 https://doi.org/10.1100/2011/289182.

Sun, B., van Dissel, D., Mo, I., Boysen, P., Haslene-Hox, H., Lund, H., 2022. Identification of novel biomarkers of inflammation in Atlantic salmon (Salmo salar L.) by a plasma proteomic approach. Dev. Comp. Immunol. 127 https://doi.org/10.1016/j.dci.2021.104268, 104268.

Taboada, X., Hermida, M., Pardo, B.G., Vera, M., Piferrer, F., Viñas, A., Bouza, C., Martínez, P., 2014. Fine mapping and evolution of the major sex determining region in turbot (Scophthalmus maximus). G3: Genes Genomes Gene. 4 (10), 1871–1880. https://doi.org/10.1534/g3.114.012328.

Tuggle, C.K., Dekkers, J.C., Reecy, J.M., 2006. Integration of structural and functional genomics. Anim. Genet. 37 (Suppl. 1), 1–6. https://doi.org/10.1111/j.1365-2052.2006.01471.x.

Valle, A., Leiro, J.M., Pereiro, P., Figueras, A., Novoa, B., Dirks, R.P.H., Lamas, J., 2020. Interactions between the parasite Philasterides dicentrarchi and the immune system of the turbot Scophthalmus maximus. A transcriptomic analysis. Biology. 9 (10), 337. https://doi.org/10.3390/biology9100337.

Vilas, R., Bouza, C., Vera, M., Millán, A., Martínez, P., 2010. Variation in anonymous and EST-microsatellites suggests adaptive population divergence in turbot. Mar. Ecol. Prog. Ser. 420, 231–239. https://doi.org/10.3354/meps08874.

Vilas, R., Vandamme, S.G., Vera, M., Bouza, C., Maes, G.E., Volckaert, F.A.M., Martínez, P., 2015. A genome scan for candidate genes involved in the adaptation of turbot (Scophthalmus maximus). Mar. Genomics 23, 77–86. https://doi.org/10.1016/j.margen.2015.04.011.

Wang, Z., Gerstein, M., Snyder, M., 2009. RNA-Seq: a revolutionary tool for transcriptomics. Nat. Rev. Genet. 10 (1), 57–63. https://doi.org/10.1038/nrg2484.

Xu, W., Zhou, H., Li, X., Wang, L., Guo, X., Yin, L., et al., 2019. C1Q/TNF-related protein 4 expression correlates with herpes simplex encephalitis progression. Ann. Transl. Med. 7 (11) https://doi.org/10.21037/atm.2019.05.01, 235–235.

Yue, F., Cheng, Y., Breschi, A., Vierstra, J., Wu, W., Ryba, T., Sandstrom, R., Ma, Z., Davis, C., Pope, B.D., Shen, Y., Pervouchine, D.D., Djebali, S., Thurman, R.E., Kaul, R., Rynes, E., Kirilusha, A., Marinov, G.K., Williams, B.A., Ren, B., 2014.

A comparative encyclopedia of DNA elements in the mouse genome. Nature 515 (7527), 355–364. https://doi.org/10.1038/nature13992.
Zhu, J., Li, C., Ao, Q., Tan, Y., Luo, Y., Guo, Y., et al., 2015. Trancriptomic profiling revealed the signatures of acute immune response in tilapia (Oreochromis niloticus) following streptococcus iniae challenge. Fish Shellfish Immunol. 46 (2), 346–353. https://doi.org/10.1016/j.fsi.2015.06.027.
Zhu, M., Foreman, D.P., O'Brien, S.A., Jin, Y., Zhang, W., 2018. Phospholipase D in TCR-mediated signaling and T cell activation. J. Immunol. 200 (6), 2165–2173. https://doi.org/10.4049/jimmunol.1701291.